Intramuscular injection of α-synuclein induces CNS α-synuclein pathology and a rapid-onset motor phenotype in transgenic mice

Amanda N. Sacino[a,b], Mieu Brooks[a,b], Michael A. Thomas[b], Alex B. McKinney[b], Sooyeon Lee[a,c], Robert W. Regenhardt[b], Nicholas H. McGarvey[b], Jacob I. Ayers[a,b], Lucia Notterpek[a,c], David R. Borchelt[a,b,c], Todd E. Golde[a,b,c,1], and Benoit I. Giasson[a,b,c,1]

[a]Department of Neuroscience, [b]Center for Translational Research in Neurodegenerative Disease, and [c]McKnight Brain Institute, University of Florida College of Medicine, Gainesville, FL 32610

Edited* by Stanley B. Prusiner, University of California, San Francisco, CA, and approved June 10, 2014 (received for review November 20, 2013)

It has been hypothesized that α-synuclein (αS) misfolding may begin in peripheral nerves and spread to the central nervous system (CNS), leading to Parkinson disease and related disorders. Although recent data suggest that αS pathology can spread within the mouse brain, there is no direct evidence for spread of disease from a peripheral site. In the present study, we show that hind limb intramuscular (IM) injection of αS can induce pathology in the CNS in the human Ala53Thr (M83) and wild-type (M20) αS transgenic (Tg) mouse models. Within 2–3 mo after IM injection in αS homozygous M83 Tg mice and 3–4 mo for hemizygous M83 Tg mice, these animals developed a rapid, synchronized, and predictable induction of widespread CNS αS inclusion pathology, accompanied by astrogliosis, microgliosis, and debilitating motor impairments. In M20 Tg mice, starting at 4 mo after IM injection, we observed αS inclusion pathology in the spinal cord, but motor function remained intact. Transection of the sciatic nerve in the M83 Tg mice significantly delayed the appearance of CNS pathology and motor symptoms, demonstrating the involvement of retrograde transport in inducing αS CNS inclusion pathology. Outside of scrapie-mediated prion disease, to our knowledge, this findiing is the first evidence that an entire neurodegenerative proteinopathy associated with a robust, lethal motor phenotype can be initiated by peripheral inoculation with a pathogenic protein. Furthermore, this facile, synchronized rapid-onset model of α-synucleinopathy will be highly valuable in testing disease-modifying therapies and dissecting the mechanism(s) that drive αS-induced neurodegeneration.

amyloid | Parkinson disease

Synucleinopathies are a group of diseases defined by the presence of amyloidogenic α-synuclein (αS) inclusions that can occur in neurons and glia of the central nervous system (CNS) (1–4). In Parkinson disease (PD), a causative role for αS has been established via the discovery of mutations in the αS gene *SNCA* resulting in autosomal-dominant PD (4–11). Although αS inclusions (e.g., Lewy bodies) are the hallmark pathology of PD, how they contribute to disease pathogenesis remains controversial (1, 3, 4, 12).

Postmortem studies have suggested that αS pathology may spread following neuroanatomical tracts (13–15) and between cells (16–18). αS pathology has also been found in the peripheral nervous system (PNS): for example, in the enteric and pelvic plexus (19, 20). And it has been suggested that αS pathology might originate in the nerves of the PNS and spread to the CNS (14). Experimentally, it has been reported that intracerebral injections of preformed amyloidogenic αS fibrils in nontransgenic (nTg) and αS transgenic (Tg) mice induce the formation of intracellular αS inclusions that appear to progress from the site of injection (21–26). Collectively, these studies support the notion that αS inclusion pathology may propagate via a prion-like conformational self-templating mechanism (27, 28). A caveat of the direct intracerebral injection of αS is that this CNS invasive surgical procedure directly alters brain homeostasis that could influence or facilitate the formation of brain pathologies, especially because incidents such as traumatic brain injury can promote the formation of αS pathology (29). Here, we report that the intramuscular (IM) injection of fibrillar (fib) αS in M83 Tg mice expressing human Ala53Thr (A53T) αS can result in the rapid and synchronized development of hind limb motor weakness and robust widespread CNS αS pathology. Additionally, similar injection into M20 Tg mice expressing human wild-type αS, which do not intrinsically develop pathology, leads to the induction of CNS αS pathology as early as 4 mo postinjection.

Results

Native M83$^{+/+}$ Tg homozygous mice show signs of motor impairment from 8 to 16 mo of age, with an arched back as the initial disease presentation that progresses to quadriparesis and a moribund state requiring euthanasia within 2 wk (30). The presentation of this phenotype is associated with the formation of αS inclusion pathology throughout most of the spinal cord and brainstem, but this phenotype never occurs spontaneously before 7 mo of age, with a median age of onset of ~12 mo of age (30, 31). We performed IM injections with various αS preparations into hind-limb muscles of 2-mo-old M83$^{+/+}$ Tg mice and monitored them for disease (Fig. 1 and Fig. S1). Initially, 10 μg of recombinant full-length mouse fibrillar αS (mfib), 21–140 fibrillar human αS (hfib21-140), human Δ71–82 αS, or lipopolysaccharide

Significance

α-Synuclein (αS) inclusions are a hallmark of many progressive neurodegenerative disorders. Previously, intracerebral injection of exogenous preformed fibrillar αS in mouse models was shown to induce neuronal αS aggregation—a finding that has been interpreted as a prion-like mechanism. We now show that αS inclusion pathology can be induced in the brain and spinal cord of αS transgenic mice by a single peripheral intramuscular injection of αS. The formation of αS inclusions occurred concurrently with the presentation of a motor impairment in mice expressing mutant Ala53Thr human αS. This new model of robust and predictable induction of αS pathology will be especially valuable to further study the pathogenic mechanisms and assessment of therapeutic interventions.

Author contributions: A.N.S., J.I.A., L.N., D.R.B., T.E.G., and B.I.G. designed research; A.N.S., M.B., M.A.T., A.B.M., and S.L. performed research; A.N.S., M.B., M.A.T., A.B.M., S.L., R.W.R., N.H.M., T.E.G., and B.I.G. analyzed data; and A.N.S., T.E.G., and B.I.G. wrote the paper.

The authors declare no conflict of interest.

*This Direct Submission article had a prearranged editor.

[1]To whom correspondence may be addressed. Email: bgiasson@ufl.edu or tgolde@ufl.edu.

This article contains supporting information online at www.pnas.org/lookup/suppl/doi:10.1073/pnas.1321785111/-/DCSupplemental.

(LPS; 25 μg) were injected bilateral in an upper hind limb muscle (biceps femoris muscles). Both mfib and hfib21-140 αS are amyloidogenic, seeding αS aggregation in vitro, in culture, and in vivo. The N-terminal truncated 21–140 αS hfib21-140 protein was used because it enables assessment of aggregation by endogenous αS by detection with N-terminal–specific αS antibodies

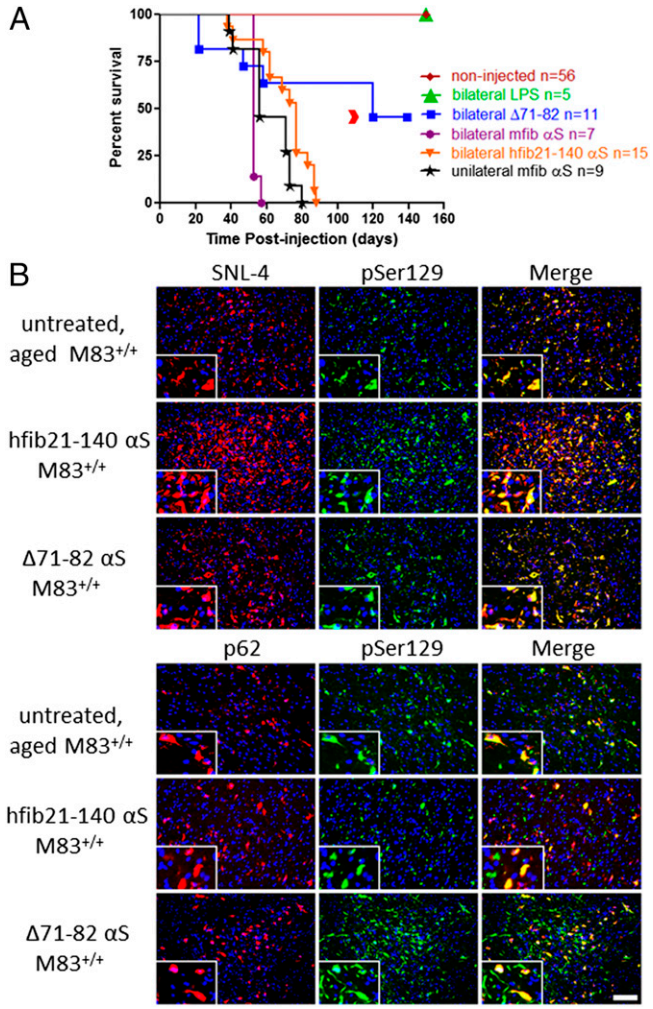

Fig. 1. αS IM injection reduces survival in M83$^{+/+}$ Tg mice. (*A*) Kaplan–Meier survival plot shows decreased survival time (due to death or euthanasia because of paralysis) for M83$^{+/+}$ Tg mice bilaterally IM-injected (biceps femoris muscle) with hfib21-140 αS compared with identical IM injection with Δ71–82 αS or LPS, and noninjected age-matched M83$^{+/+}$ Tg mice. Median times to moribund state were as follows: within 88 dpi (median 62 dpi) for mice IM-injected bilaterally with fibrillar (mfib and hfib21-140) αS (n = 22); within 80 dpi (median 56 dpi) for those injected unilaterally with mfib αS (n = 9); and within 120 dpi for phenotypic mice injected with Δ71–82 αS (n = 6; the red arrowhead indicates time to moribund state for the two mice with foot drop/paralysis). Mice IM-injected with LPS (n = 5) and noninjected M83$^{+/+}$ Tg mice (n = 56) remained disease free ($P < 0.0001$; χ^2, 123.7; df, 5). All mice IM-injected bilaterally (biceps femoris muscle) with mfib αS died or had to be killed due to paralysis within 57 dpi (n = 7; median 53 dpi) and with hfib21-140 αS within 88 dpi (n = 14; median 77 dpi) ($P < 0.01$; χ^2, 10.62; df, 1). (*B*) Double immunofluorescence analyses of midbrain region from an untreated, aged (11-mo-old) movement-impaired M83$^{+/+}$ Tg mouse, an M83$^{+/+}$ Tg mouse that is 2 mo postinjection with 10 μg of hfib21-140 αS, and an M83$^{+/+}$ Tg mouse that is 4 mo postinjection with 10 μg of Δ71–82 αS. Anti-pSer129–labeled αS inclusions (green) were also detected with the anti–N-terminal αS antibody SNL-4 (red, *Upper*) and with an antibody to p62, a nonspecific intracellular inclusion marker (red, *Lower*). Tissue sections were counterstained with DAPI (blue). (Scale bar: *B*, 100 μm; *Insets*, 25 μm.)

(32–35). Nonamyloidogenic human Δ71–82 αS has a deletion of αS required for amyloid formation and lacks the ability to form or seed αS amyloid in vitro and in cultured cells under relatively physiologic conditions (32, 33, 36, 37). IM injection of human Δ71–82 αS was used to test the hypothesis that induction of αS pathology occurs through amyloidogenic conformational templating. LPS was used as a control for potential inflammatory effects induced by αS (38–40). Forty to 90 d post IM injection (dpi) with hfib21-140 or mfib αS, M83$^{+/+}$ Tg mice developed a unilateral foot drop that progressed rapidly to a bilateral foot drop followed by full hind limb paralysis within a week of onset (Fig. 1 and Movie S1). Mice reached a terminal state at a median of 53 d and 77 d postinjection for mfib and hfib21-140 αS, respectively. Although M83$^{+/+}$ Tg mice injected with mfib αS showed an early disease onset (Fig. 1 and Table S1), there was no detectable difference in disease progression. Unilateral IM injection of mfib αS in a lower hind limb muscle (gastrocnemius) of M83$^{+/+}$ Tg mice also resulted in the same induction of phenotype, albeit delayed compared with the bilateral IM-injected mice (Fig. 1 and Table S1).

Mice injected with fibrillar αS developed αS inclusion pathology that was nearly indistinguishable morphologically in anatomic distribution from that seen in aged (>8 mo old) untreated M83$^{+/+}$ Tg mice (Fig. 2 and Fig. S1) (30). In contrast to IM injection of fibrillar αS, no αS inclusion pathology or any overt behavioral changes were observed in mice injected with LPS (Fig. 1 and Table S1). αS inclusion pathology in mice injected with preformed fibrillar αS was robust in the spinal cord, brainstem, and midbrain structures, but sparse in the cortex (Fig. 2). There was a high density of αS pathology in the midbrain, but inclusions were rarely observed in dopaminergic neurons (Fig. S2). The αS inclusions were composed of endogenous αS, as shown by reactivity with anti–N-terminal αS antibodies Syn506 and SNL-4, and they are also strongly reactive with p62 antibodies, a nonspecific marker of intracellular protein aggregates (Fig. 1 and Fig. S1) (41). αS inclusions were not found in the sciatic nerve or muscle injection site (Fig. S3). It is possible that the paucity of αS aggregates at these sites is due to only a small quantity of αS accumulating at these compartments, or that they have been degraded or even truncated by the time of examination. Nevertheless, these data indicate that a peripheral IM hfib21-140 or mfib injection dramatically accelerates onset of disease in the M83$^{+/+}$ Tg model, with complete penetrance in this study.

Compared with results with amyloidogenic forms of αS, IM injection of the nonamyloidogenic Δ71–82 resulted in delayed onset of disease and incomplete penetrance of the accelerated pathology. Six of 11 Δ71–82 αS IM-injected M83$^{+/+}$ Tg mice became moribund, with 2 of these 6 developing a motor phenotype at 120 dpi indistinguishable from that observed in the fib-αS–injected mice. The phenotype in the additional 4 moribund mice was distinct as these mice had a more generalized muscle weakness but without hind leg drop foot. The 2 mice with the hind leg paralysis plus foot drop and 3 other mice killed at 139 dpi without motor signs showed αS pathology similar to untreated, aged M83$^{+/+}$ Tg mice (Figs. 1 and 2, Fig. S1, and Table S1). In contrast, the additional 4 moribund M83$^{+/+}$ Tg mice IM injected with Δ71–82 αS did not present with any detectable αS inclusion pathology.

To compare induction of a motor phenotype and αS pathology in a model with lower endogenous expression of αS, we performed the same IM injections in M83$^{+/-}$ Tg hemizygous mice. The M83$^{+/-}$ Tg mice express A53T human αS throughout the neuroaxis similarly to M83$^{+/+}$ Tg mice but at ∼60% the expression level, and they do not endogenously develop αS inclusion pathology or motor impairments before 18 mo of age (30). We initially performed bilateral IM injections of fibrillar αS in M83$^{+/-}$ Tg mice to test that the same motor phenotype could be induced (Fig. 3 and Table S1). Bilateral or unilateral injection of fib αS in M83$^{+/-}$ Tg mice resulted in an identical progressive degenerative motor phenotype to that seen in injected

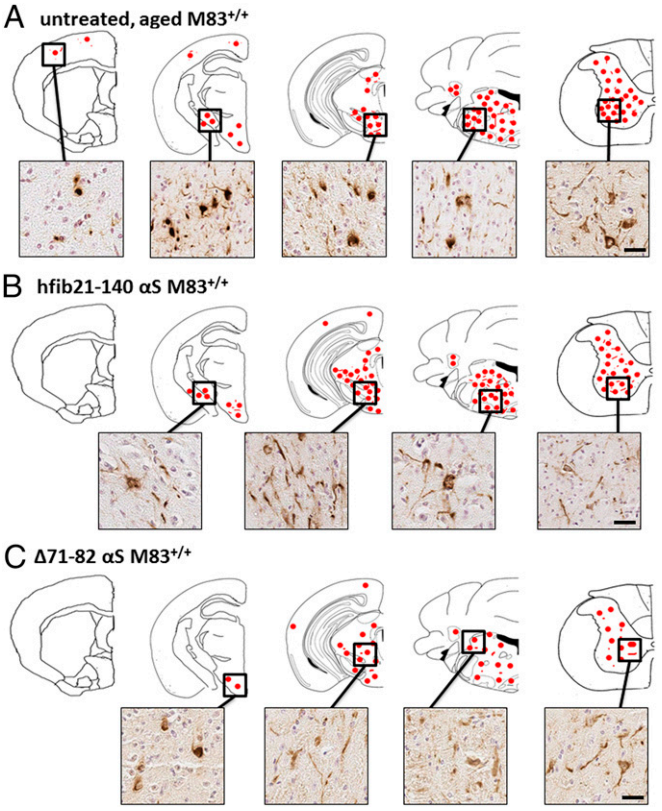

Fig. 2. αS pathology in M83$^{+/+}$ Tg mice IM-injected with αS is similar to that seen in untreated, aged M83$^{+/+}$ Tg mice. Schematic representation of the distribution of CNS αS inclusion pathology (depicted as red dots) detected by pSer129 staining for hyperphosphorylated αS and that was also confirmed with Syn506 staining, an anti–N-terminal αS antibody that conformationally detects αS inclusions (57) and p62, an antibody that nonspecifically recognizes intracellular protein aggregates (41) (Fig. S1). Representative immunohistochemical (IHC) images of αS inclusion pathology from various regions are shown. (*A*) αS inclusion pathology distribution in untreated, aged (>11 mo old) movement-impaired M83$^{+/+}$ Tg mice. αS pathology is abundant in the spinal cord, brainstem, and midbrain areas and rare in the cortex and absent in the hippocampus (30). M83$^{+/+}$ Tg mice IM-injected with 10 μg of hfib21-140 αS (*B*) or 10 μg of Δ71–82 αS (*C*) at 4 mo of age and 6 mo of age, respectively, depicted similar bilateral pathology (also see Fig. S1). (Scale bars: 50 μm.)

M83$^{+/+}$ Tg mice, but with a delayed onset (Fig. 3*A* and Table S1). The distribution and density of αS pathology induced in all M83$^{+/-}$ Tg mice at the time of demise was also identical to that seen in M83$^{+/+}$ Tg mice.

To determine whether induction of αS pathology in the brain and spinal cord postinjection was due to neuroinvasion of the injected αS via retrograde transport through the sciatic nerve (the major nerve that innervates lower leg muscles), we performed complete transection of the left sciatic nerve 3 d before injection of 10 μg of mfib αS in the left gastrocnemius muscle in M83$^{+/-}$ Tg mice. Sciatic nerve transection significantly delayed and, in some mice, perhaps completely prevented the CNS neuroinvasion of the IM-injected αS (Fig. 3 and Table S1). Three of the seven mice on which we performed this procedure still developed motor impairment, with CNS αS pathology identical to mice without nerve transection, but the onset was dramatically delayed (Fig. 3 and Table S1). Four of the seven mice that had sciatic nerve transection followed by fibrillar αS muscle injection showed no motor deficits 200 d post IM injection. These data implicate retrograde axonal transport as the predominant mechanism for CNS neuroinvasion of the IM-injected αS.

IM αS injection studies were also conducted in M20 Tg mice that overexpress human wild-type αS but never intrinsically develop a phenotype or αS inclusion pathology (30, 31). Because M20$^{+/-}$ Tg hemizygous mice express human αS at similar levels and neuroanatomical distribution as M83$^{+/+}$ Tg mice (30), we performed all these studies with M20$^{+/-}$ Tg mice for more appropriate comparison. In contrast to the M83 Tg mice, IM-injected M20$^{+/-}$ Tg mice did not develop any overt motor phenotype; however, beginning at 4 mo postinjection, rare αS inclusions were detected in the spinal cord αS antibodies, but these aggregates were not detected with antibodies to the general inclusion marker, p62 (41). At 8 and 12 mo after IM injection of hfib21-140 αS, induction of αS inclusion pathology was observed in the CNS, albeit less robustly than in M83 Tg mice (Fig. 4, Fig. S1, and Table S2). αS pathology in hfib21-140 αS IM-injected M20$^{+/-}$ Tg mice was predominantly found in neuronal processes and some cell bodies in the periaqueductal gray area of the midbrain and in white and gray matter at all levels of the spinal cord. Although αS pathology was found in the midbrain brain, inclusions were rarely found in dopaminergic neurons

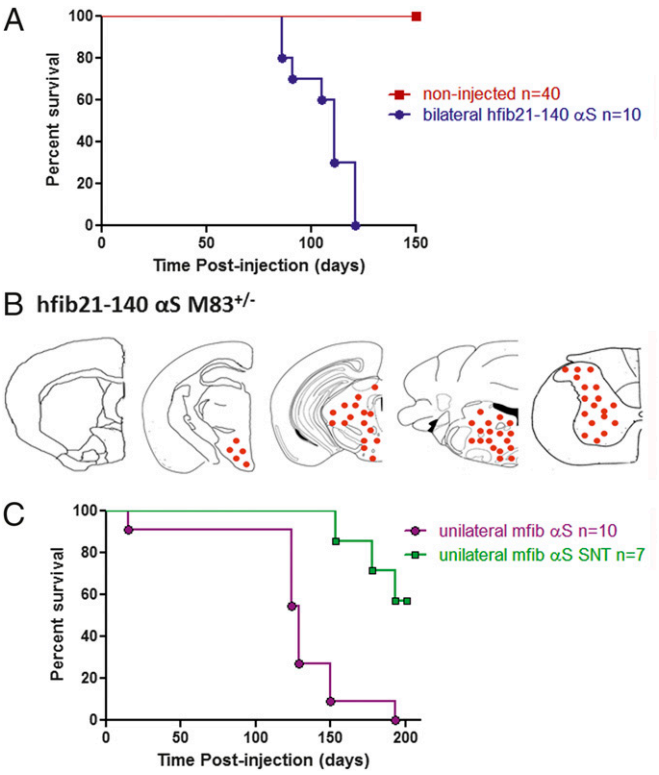

Fig. 3. αS IM injection reduces survival in M83$^{+/-}$ Tg mice. (*A*) Kaplan–Meier survival plot shows a decreased time to terminal state (killed due to paralysis) for M83$^{+/-}$ Tg mice injected bilaterally (gastrocnemius muscle) with 10 μg of hfib21-140 αS (n = 10) compared with noninjected M83$^{+/-}$ Tg mice (n = 40). All injected mice reached a terminal state (paralysis) within 121 d postinjection (median 111 d; $P < 0.0001$; χ^2, 67.58; df, 1). (*B*) Schematic representation of the distribution of CNS αS inclusion pathology (depicted as red dots) in M83$^{+/-}$ Tg mice detected by pSer129 staining for hyperphosphorylated αS and that was also confirmed with Syn506 staining, an anti–N-terminal αS antibody that conformationally detects αS inclusions (54) and p62, an antibody that nonspecifically recognizes intracellular protein aggregates (41). (*C*) All M83$^{+/-}$ Tg mice unilaterally injected (gastrocnemius muscle) with 10 μg of mfib αS reached a terminal state (killed due to paralysis) within 193 d postinjection (median 129 d). However, in M83$^{+/-}$ Tg mice in which the sciatic nerve was transected (3 d) preinjection, the time to terminal state was delayed past the window seen with the nontransected controls ($P < 0.001$; χ^2, 12.01; df, 1).

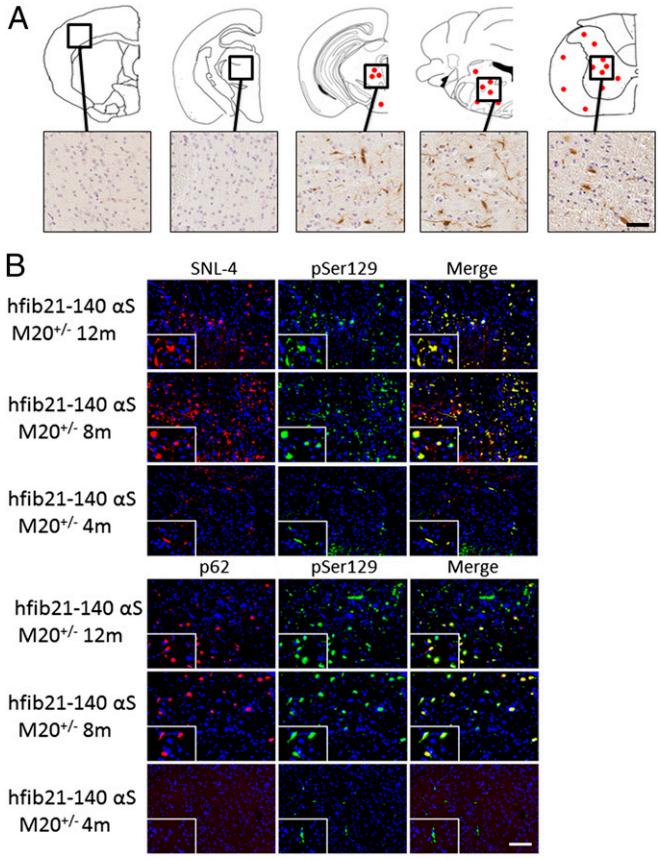

Fig. 4. Induction of αS pathology post IM injection of 10 μg of hfib21-140 αS in $M20^{+/-}$ Tg mice. (*A*) Schematic summary of rostral-caudal αS pathology distribution in $M20^{+/-}$ Tg mice 12 mo after bilateral IM injection with hfib21-140 αS that is detected by a panel of αS inclusion markers. A moderate density of αS pathology was seen throughout the spinal cord, brainstem, and midbrain, with no pathology in the striatum, hippocampus, or cortex. The hyperphosphorylated αS inclusions were also detected by Syn506, an anti–N-terminal αS antibody that conformationally detects αS inclusions (57), and p62, an antibody that nonspecifically recognizes intracellular protein aggregates (41). Equivalent density and distribution of αS pathology was observed bilaterally. (*B*) Double immunofluorescence analyses of lumbar spinal cord sections from M20 Tg mice that are 12 mo, 8 mo, and 4 mo postinjection with 10 μg of hfib21-140 αS. pSer129 αS inclusions (green) are also labeled with SNL-4, an anti–N-terminal αS antibody (red, *Upper*), and with an antibody to p62, a nonspecific intracellular inclusion marker (red, *Lower*), at 12 mo and 8 mo postinjection. At 4 mo postinjection, pSer129-labeled αS inclusions were also detected with SNL-4, but they were not detected with p62 antibodies. Tissue sections were counterstained with DAPI (blue). (Scale bars: *A*, 50 μm; *B*, 100 μm; *Insets*, 25 μm.)

(Fig. S2). αS inclusions were not found in the sciatic nerve near the muscle injection site (Fig. S3).

We performed similar IM injections of fibrillar αS in non-transgenic (nTg) mice (C3H/C57BL6 strain background that is the same as M83 and M20 Tg mice) as well as in $SNCA^{-/-}$ mice (Table S3). No mice from these cohorts developed a motor phenotype or αS pathology at 12 mo postinjection (Table S3). The paucity of induction of CNS αS pathology in nTg mice is consistent with retrograde axonal transport as a major mode transmission/induction and the low level of expression of endogenous αS in the sciatic nerve and the spinal cord (Fig. S3) (42).

To try to understand the physiological changes associated with αS inclusion pathology and the motor impairments in αS Tg mice IM injected with αS, we investigated alterations in the neuroinflammatory state. Tissue sections from all $M83^{+/+}$ Tg injected mice were stained for the astrocyte marker, GFAP, and the microglia marker, Iba-1 (Fig. S4). In untreated, aged $M83^{+/+}$ Tg mice with CNS αS inclusion pathology, there was concurrent astrogliosis in the areas with αS pathology; however, there was little increase in microgliosis. Interestingly, $M83^{+/+}$ Tg mice IM injected with LPS or Δ71–82 αS that did not develop αS pathology even up to 4 mo postinjection did not show elevated levels of astrogliosis or microgliosis. On the other hand, $M83^{+/+}$ Tg mice injected with Δ71–82 αS or fibrillar αS (no differences seen between mfib or hfib21-140, bilateral or unilateral injections) that developed αS pathology also showed massive astrogliosis in the areas with αS inclusion pathology as seen in aged $M83^{+/+}$ Tg mice that develop a motor phenotype, as well as elevated microgliosis in the areas with αS pathology. Comparatively, no elevated neuroinflammatory response in $M20^{+/-}$ Tg mice was observed at any time point postinjection compared with PBS-injected $M20^{+/-}$ Tg mice (Table S2) and naive $M20^{+/-}$ Tg mice controls. Collectively, these data indicate that IM injections in $M83^{+/+}$ Tg mice leading to the development of αS pathology are associated with increased microgliosis and astrogliosis.

Interestingly, αS pathology in the brain and spinal cord of αS-IM–injected M20 and M83 Tg mice was found in both astrocytes and neurons; however, although αS pathology was readily found in motor neurons in the ventral horn of the spinal cord in M83 Tg mice, they were less frequently seen in M20 Tg mice with αS pathology (Fig. S5). As the development of αS pathology in M83 Tg motor neurons could contribute to the development of the progressive motor phenotype seen in these mice, we quantified the number of motor neurons and found that there is a 76% loss of motor neurons in injected M83 Tg mice ($M83^{+/-}$ Tg mice average number of motor neurons per section was 1.8 ± 0.5 compared with an average of 7.7 ± 1.0 motor neurons per section in age-matched, naive nTg mice; $P < 0.0001$). In a previous characterization of the M83 Tg mice, it has been shown that untreated, motor-impaired aged M83 Tg mice do not have statistically different levels of motor neurons compared with nTg mice (30); therefore, this loss of motor neuron is related to the injection of exogenous αS. We additionally found that the loss of motor neurons in phenotypic M83 Tg mice corresponded to a 72% decrease in the innervation of the neuromuscular junction (NMJ) in the digitorum brevis muscles, which are solely innervated by a branch of the sciatic nerve (average ratio of innervated NMJ in injected $M83^{+/-}$ Tg mice is 0.25 ± 0.09 compared with age-matched, naive $M83^{+/-}$ Tg mice with 0.92 ± 0.07; $P < 0.0001$) (Fig. S6). Collectively, these data point to the progressive induction of αS pathology in ventral horn motor neurons, with the demise of these cells as a causative factor for inciting the motor dysfunction seen in M83 Tg mice IM injected with αS.

Discussion

Our findings show that αS pathology in the CNS can be efficiently induced with peripheral injections of amyloidogenic αS and less efficiently with "non-amyloidogenic" αS in M83 Tg mice. In both cases, αS pathology is associated with a rapidly progressive motor phenotype that is subtly distinct from that in untreated, aged M83 Tg mice due to the initial foot drop presentation and the heightened neuroinflammatory response. From our findings, IM injections appear to induce a more rapid lethal motor phenotype (50–120 d incubation time) than reported in some studies where either homozygous or hemizygous M83 Tg were intracerebrally inoculated with CNS extracts from symptomatic M83 Tg (~200 d incubation time) (23, 24). However, Luk et al. (21) reported that, in similar M83 Tg CNS extract transmission studies or with intracerebral injection of recombinant fib αS in homozygous M83 Tg mice, the incubation time to cause motor impairments was closer to what we observed resulting from IM injection of fib αS (i.e., ~100 d) (21). Nevertheless, the relative rapid induction of widespread CNS αS pathology from the peripheral injection of fib αS in our IM experimental paradigm is in contrast to the studies of peripheral inoculations of scrapie prions where the incubation times are

always longer than those found after intracerebral inoculation (43). It is possible that some unique properties of αS, such as vesicle binding and more rapid retrograde transport, facilitate this process. However, more rigorously controlled parallel intracerebral versus IM inoculation studies are needed before definite comparison of injection sites on incubation lag time to disease state can be established. All of the αS transmission studies performed by different groups using M83 Tg mice were conducted with different forms and amounts of inoculums. Thus, varying amounts of transmissive αS likely used in these different studies confounds the direct comparison of incubation time needed to lead to disease from different sites of injections.

αS IM-injected M83 Tg mice also have a large decrease in spinal cord motor neurons and reductions in innervated NMJs in muscle innervated by the sciatic nerve. The delay and attenuation of disease-induction results observed in the sciatic nerve transection studies provide strong support that retrograde transport of exogenous αS to the spinal cord is a primary mechanism of CNS neuroinvasion. It is not completely clear how αS CNS pathology was still induced in a subset of mice with sciatic nerve transection. The sciatic nerve is the major nervous system connection between the spinal cord and the lower hind leg muscles, but there are other minor nerves that may also lead to retrograde transport. The site of muscle injection (gastrocnemius muscle) is far from the site of transection at the level of the thigh, but it is possible that some injected αS was able to remain in the muscle long enough for some nerve sprouting to occur. Furthermore, it is possible that some of the injected αS was able to enter the CNS via other systemic circulation mechanism(s) or that other secondary induction mechanism(s) can indirectly contribute to the induced CNS αS pathology.

The finding that αS inclusion pathology was also induced in glial cells in the spinal cord indicates that induction/spread does not in all cases follow neuroanatomical pathways. It is also intriguing that no αS inclusions were observed in the sciatic nerve of any of the injected mice. This finding suggests that (*i*) the retrograde transport in this nerve may be too rapid for inclusion formation to occur, (*ii*) αS being transported via retrograde transport is in a state such that it is not available to polymerize into inclusions, or (*iii*) the concentration of αS in the sciatic nerve is not sufficient for inclusion formation.

We have additionally shown that similar injections of exogenous αS into M20 Tg mice induce the formation of CNS αS inclusion pathology. However, this process is much slower than in M83 Tg mice. The specific factors that account for the difference between these two lines remain enigmatic but these components may hold important clues to how to halt disease progression in humans. The M20 Tg mice express wild-type human αS whereas the M83 Tg mice express A53T human αS, which have a greater propensity to aggregate into amyloid in vitro (44–46). This difference may contribute to the increased vulnerability of M83 Tg mice, but other still unknown synergistic mechanisms may also be more pronounced in M83 Tg mice.

Peripheral injections of αS aggregates into nTg mice did not produce any obvious neuropathological or behavioral abnormality. This finding is similar to another study of intranasal administration of αS (25). Recently, Rey et al. (47) have shown that injection of exogenous monomeric or aggregated αS in the mouse olfactory bulb can result in the transport to neurons of neuroanatomically connected brain regions, but the injected proteins had a short half-life (less than 72 h) and no induction of αS pathology was observed (47). Thus, it appears that the higher endogenous levels of αS in primed animals greatly accentuate the experimental peripheral induction of αS pathology. Indeed, it has been recently shown that i.p. administration of exogenous tau into transgenic mice overexpressing human mutant P301L tau results in the induction of an intracerebral tauopathy at 9 mo postinjection (48). Similarly, i.p. injections of brain extracts laden with Aβ aggregates into transgenic mice expressing the amyloid precursor protein also induced cerebral β-amyloidosis (49, 50). Overall, our experience has been that using transgenic mice in exogenous seeding experiments greatly enhances the probability of transmitting pathogenic protein aggregation.

Our findings also highlight the fact, as we have noted elsewhere (51, 52), that there seem to be significant differences in the susceptibility of different models to induction of pathology. Mice expressing A53T αS are susceptible to rapid onset of a neurodegenerative phenotype associated with motor neuron death and a decrease in NMJ integrity in the affected limbs. The time-course studies in M20 Tg mice show a progressive spread of αS, albeit less efficient, from the spinal cord to the brain in the absence of a neuroinflammatory response. Studies using this model may in turn provide more direct evidence for the prion-like spread of αS pathology, without the exacerbating effects of multiple synergistic mechanisms.

Previous experimental studies have provided evidence for in vivo prion-like spread of αS pathology (21–26); however, several findings here, and in other recent studies from our group, suggest that additional nonexclusive mechanisms inducing or promoting αS inclusion pathology formation should be considered (33, 51–53). Indeed, (*i*) the distribution of αS pathology in M83 Tg mice IM injected with various forms of αS was identical to that seen in untreated, aged M83 Tg mice, (*ii*) IM injection of a nonamyloidogenic form of αS (Δ71–82) induced CNS αS inclusion pathology, albeit less efficiently than fibrillar αS, and (*iii*) there were significant increases of both astrogliosis and microgliosis associated with the regions where abundant αS pathology was induced.

Our finding using of Δ71–82 αS suggests that the amyloidogenic form of αS is not required for the induction of αS pathology and a motor phenotype and that mechanism(s) besides prion-like conformational templating may contribute to induction of disease. Under experimental native and physiological conditions, Δ71–82 αS is refractory to amyloid formation, and it does not promote or influence amyloid formation of full-length αS (32, 33, 36, 37); however, under nonphysiological conditions (i.e., the presence of SDS), it can be artificially induced to form amyloid fibrils (54). At present, we cannot completely exclude the possibility that a small amount of soluble Δ71–82 αS may spontaneously form amyloid seeds in vivo. It is possible that additional factors, analogous to the Protein X in prion disease (55), absent in in vitro systems could facilitate the conversion of the nonamyloidogenic αS to an amyloidogenic form in vivo. Furthermore, amyloidogenicity is not a prerequisite for all forms of self-templating propagation of protein aggregation, and it may be that Δ71–82 αS is directly inducing structural changes in endogenous αS, leading to aggregation by a nonamyloidogenic mechanism.

Our ability to now synchronously and rapidly induce a motor phenotype and αS pathology by a peripheral injection of αS may prove invaluable in future studies exploring mechanisms of pathology induction and αS toxicity and may extend recent studies showing rapid induction following intracerebral inoculation (21–26). Our finding that disease onset in M83 Tg mice can be shortened, predicted, and synchronized through a simple manipulation provides a valuable model to accelerate studies designed to fully understand the mechanisms underlying induction of the inclusion pathology and motor phenotype, but also to enable much more rapid and cost-effective preclinical testing of novel PD therapies.

Materials and Methods

Mice Husbandry and Procedures. All procedures were performed according to the National Institutes of Health Guide for the Care and Use of Experimental Animals and were approved by the University of Florida Institutional Animal Care and Use Committee. M83 Tg mice expressing human αS with the A53T mutation or M20 Tg mice expressing wild-type human αS drive by the mouse prion protein promoter were previously described (30, 31). *SNCA*$^{-/-}$ mice (56) were obtained from The Jackson Laboratory, and C3H/C57BL6 nTg mice were obtained from Harlan Labs. All animals were maintained on ad libitum food and water with a 12 h light/dark cycle.

Intramuscular Injection into M83 Tg or M20 Tg Mice. Bilateral injection of αS proteins and lipopolysaccharide (LPS; Sigma-Aldrich) or PBS control was performed by inserting the needle ∼1 mm deep into the biceps femoris or gastrocnemius muscle (as summarized in Tables S1–S3). Mice at 2 mo of age were anesthetized with isoflurane (1–5%) inhalation. Injections were made using a 10-μL Hamilton syringe with a 25-gauge needle. Different syringes were used for each type of inoculum to prevent any contamination. Post-injection, mice were placed on a heating pad for recovery before being returned to their home cage. Some $M83^{+/+}$ αS Tg mice and $M83^{+/-}$ αS Tg mice were also unilaterally injected with mouse αS fibrils in the left gastrocnemius muscle. For a subset of these $M83^{+/-}$ αS Tg mice, the left sciatic nerve was completely severed at the level of the thigh 3 d before muscle injection.

Addition information on other materials and methods are included in *SI Materials and Methods*.

ACKNOWLEDGMENTS. This work was supported by an Ellison Medical Foundation Senior Scholar Award (to T.E.G.), a Wilder Family Fellowship (to A.N.S.), the Santa Fe HealthCare Alzheimer's Disease Research Center (D.R.B.), grants from the Michael J. Fox Foundation and the National Parkinson Foundation, and funding from the University of Florida.

1. Cookson MR (2005) The biochemistry of Parkinson's disease. *Annu Rev Biochem* 74: 29–52.
2. Gasser T (2009) Mendelian forms of Parkinson's disease. *Biochim Biophys Acta* 1792(7): 587–596.
3. Goedert M (2001) Alpha-synuclein and neurodegenerative diseases. *Nat Rev Neurosci* 2(7):492–501.
4. Waxman EA, Giasson BI (2009) Molecular mechanisms of alpha-synuclein neurodegeneration. *Biochim Biophys Acta* 1792(7):616–624.
5. Polymeropoulos MH, et al. (1997) Mutation in the alpha-synuclein gene identified in families with Parkinson's disease. *Science* 276(5321):2045–2047.
6. Krüger R, et al. (1998) Ala30Pro mutation in the gene encoding alpha-synuclein in Parkinson's disease. *Nat Genet* 18(2):106–108.
7. Zarranz JJ, et al. (2004) The new mutation, E46K, of alpha-synuclein causes Parkinson and Lewy body dementia. *Ann Neurol* 55(2):164–173.
8. Farrer M, et al. (2004) Comparison of kindreds with parkinsonism and alpha-synuclein genomic multiplications. *Ann Neurol* 55(2):174–179.
9. Singleton AB, et al. (2003) alpha-Synuclein locus triplication causes Parkinson's disease. *Science* 302(5646):841.
10. Kiely AP, et al. (2013) α-Synucleinopathy associated with G51D SNCA mutation: A link between Parkinson's disease and multiple system atrophy? *Acta Neuropathol* 125(5): 753–769.
11. Proukakis C, et al. (2013) A novel α-synuclein missense mutation in Parkinson disease. *Neurology* 80(11):1062–1064.
12. Dawson T, Mandir A, Lee M (2002) Animal models of PD: Pieces of the same puzzle? *Neuron* 35(2):219–222.
13. Braak H, Rüb U, Gai WP, Del Tredici K (2003) Idiopathic Parkinson's disease: possible routes by which vulnerable neuronal types may be subject to neuroinvasion by an unknown pathogen. *J Neural Transm* 110(5):517–536.
14. Braak H, et al. (2006) Stanley Fahn Lecture 2005: The staging procedure for the inclusion body pathology associated with sporadic Parkinson's disease reconsidered. *Mov Disord* 21(12):2042–2051.
15. Braak H, et al. (2003) Staging of brain pathology related to sporadic Parkinson's disease. *Neurobiol Aging* 24(2):197–211.
16. Kordower JH, Chu Y, Hauser RA, Freeman TB, Olanow CW (2008) Lewy body-like pathology in long-term embryonic nigral transplants in Parkinson's disease. *Nat Med* 14(5):504–506.
17. Li JY, et al. (2008) Lewy bodies in grafted neurons in subjects with Parkinson's disease suggest host-to-graft disease propagation. *Nat Med* 14(5):501–503.
18. Li JY, et al. (2010) Characterization of Lewy body pathology in 12- and 16-year-old intrastriatal mesencephalic grafts surviving in a patient with Parkinson's disease. *Mov Disord* 25(8):1091–1096.
19. Wakabayashi K, Mori F, Tanji K, Orimo S, Takahashi H (2010) Involvement of the peripheral nervous system in synucleinopathies, tauopathies and other neurodegenerative proteinopathies of the brain. *Acta Neuropathol* 120(1):1–12.
20. Braak H, de Vos RA, Bohl J, Del Tredici K (2006) Gastric alpha-synuclein immunoreactive inclusions in Meissner's and Auerbach's plexuses in cases staged for Parkinson's disease-related brain pathology. *Neurosci Lett* 396(1):67–72.
21. Luk KC, et al. (2012) Intracerebral inoculation of pathological α-synuclein initiates a rapidly progressive neurodegenerative α-synucleinopathy in mice. *J Exp Med* 209(5): 975–986.
22. Luk KC, et al. (2012) Pathological α-synuclein transmission initiates Parkinson-like neurodegeneration in nontransgenic mice. *Science* 338(6109):949–953.
23. Watts JC, et al. (2013) Transmission of multiple system atrophy prions to transgenic mice. *Proc Natl Acad Sci USA* 110(48):19555–19560.
24. Mougenot AL, et al. (2012) Prion-like acceleration of a synucleinopathy in a transgenic mouse model. *Neurobiol Aging* 33(9):2225–2228.
25. Masuda-Suzukake M, et al. (2013) Prion-like spreading of pathological α-synuclein in brain. *Brain* 136(Pt 4):1128–1138.
26. Recasens A, et al. (2014) Lewy body extracts from Parkinson disease brains trigger α-synuclein pathology and neurodegeneration in mice and monkeys. *Ann Neurol* 75(3):351–362.
27. Jucker M, Walker LC (2013) Self-propagation of pathogenic protein aggregates in neurodegenerative diseases. *Nature* 501(7465):45–51.
28. Polymenidou M, Cleveland DW (2012) Prion-like spread of protein aggregates in neurodegeneration. *J Exp Med* 209(5):889–893.
29. Uryu K, et al. (2003) Age-dependent synuclein pathology following traumatic brain injury in mice. *Exp Neurol* 184(1):214–224.
30. Giasson BI, et al. (2002) Neuronal alpha-synucleinopathy with severe movement disorder in mice expressing A53T human alpha-synuclein. *Neuron* 34(4):521–533.
31. Emmer KL, Waxman EA, Covy JP, Giasson BI (2011) E46K human alpha-synuclein transgenic mice develop Lewy-like and tau pathology associated with age-dependent, detrimental motor impairment. *J Biol Chem* 286(40):35104–35118.
32. Luk KC, et al. (2009) Exogenous alpha-synuclein fibrils seed the formation of Lewy body-like intracellular inclusions in cultured cells. *Proc Natl Acad Sci USA* 106(47): 20051–20056.
33. Sacino AN, et al. (2013) Conformational templating of α-synuclein aggregates in neuronal-glial cultures. *Mol Neurodegener* 8:17.
34. Waxman EA, Giasson BI (2010) A novel, high-efficiency cellular model of fibrillar alpha-synuclein inclusions and the examination of mutations that inhibit amyloid formation. *J Neurochem* 113(2):374–388.
35. Waxman EA, Giasson BI (2011) Induction of intracellular tau aggregation is promoted by α-synuclein seeds and provides novel insights into the hyperphosphorylation of tau. *J Neurosci* 31(21):7604–7618.
36. Giasson BI, Murray IV, Trojanowski JQ, Lee VMY (2001) A hydrophobic stretch of 12 amino acid residues in the middle of alpha-synuclein is essential for filament assembly. *J Biol Chem* 276(4):2380–2386.
37. Waxman EA, Mazzulli JR, Giasson BI (2009) Characterization of hydrophobic residue requirements for alpha-synuclein fibrillization. *Biochemistry* 48(40):9427–9436.
38. Kim C, et al. (2013) Neuron-released oligomeric α-synuclein is an endogenous agonist of TLR2 for paracrine activation of microglia. *Nat Commun* 4:1562.
39. Fellner L, et al. (2013) Toll-like receptor 4 is required for α-synuclein dependent activation of microglia and astroglia. *Glia* 61(3):349–360.
40. Codolo G, et al. (2013) Triggering of inflammasome by aggregated α-synuclein, an inflammatory response in synucleinopathies. *PLoS ONE* 8(1):e55375.
41. Kuusisto E, Parkkinen L, Alafuzoff I (2003) Morphogenesis of Lewy bodies: Dissimilar incorporation of alpha-synuclein, ubiquitin, and p62. *J Neuropathol Exp Neurol* 62(12):1241–1253.
42. Giasson BI, Duda JE, Forman MS, Lee VMY, Trojanowski JQ (2001) Prominent perikaryal expression of α- and β-synuclein in neurons of dorsal root ganglion and in medullary neurons. *Exp Neurol* 172(2):354–362.
43. Kimberlin RH, Cole S, Walker CA (1987) Pathogenesis of scrapie is faster when infection is intraspinal instead of intracerebral. *Microb Pathog* 2(6):405–415.
44. Giasson BI, Uryu K, Trojanowski JQ, Lee VMY (1999) Mutant and wild type human alpha-synucleins assemble into elongated filaments with distinct morphologies in vitro. *J Biol Chem* 274(12):7619–7622.
45. Conway KA, Harper JD, Lansbury PT (1998) Accelerated in vitro fibril formation by a mutant alpha-synuclein linked to early-onset Parkinson disease. *Nat Med* 4(11): 1318–1320.
46. Narhi L, et al. (1999) Both familial Parkinson's disease mutations accelerate alpha-synuclein aggregation. *J Biol Chem* 274(14):9843–9846.
47. Rey NL, Petit GH, Bousset L, Melki R, Brundin P (2013) Transfer of human α-synuclein from the olfactory bulb to interconnected brain regions in mice. *Acta Neuropathol* 126(4):555–573.
48. Clavaguera F, et al. (2014) Peripheral administration of tau aggregates triggers intracerebral tauopathy in transgenic mice. *Acta Neuropathol* 127(2):299–301.
49. Eisele YS, et al. (2010) Peripherally applied Abeta-containing inoculates induce cerebral β-amyloidosis. *Science* 330(6006):980–982.
50. Eisele YS, et al. (2009) Induction of cerebral β-amyloidosis: Intracerebral versus systemic Abeta inoculation. *Proc Natl Acad Sci USA* 106(31):12926–12931.
51. Sacino AN, et al. (2013) Induction of CNS α-synuclein pathology by fibrillar and non-amyloidogenic recombinant α-synuclein. *Acta Neuropathol Commun* 1(1):38.
52. Sacino AN, et al. (2014) Amyloidogenic α-synuclein seeds do not invariably induce rapid, widespread pathology in mice. *Acta Neuropathol* 127(5):645–665.
53. Golde TE, Borchelt DR, Giasson BI, Lewis J (2013) Thinking laterally about neurodegenerative proteinopathies. *J Clin Invest* 123(5):1847–1855.
54. Rivers RC, et al. (2008) Molecular determinants of the aggregation behavior of alpha- and beta-synuclein. *Protein Sci* 17(5):887–898.
55. Telling GC, et al. (1995) Prion propagation in mice expressing human and chimeric PrP transgenes implicates the interaction of cellular PrP with another protein. *Cell* 83(1): 79–90.
56. Abeliovich A, et al. (2000) Mice lacking alpha-synuclein display functional deficits in the nigrostriatal dopamine system. *Neuron* 25(1):239–252.
57. Waxman EA, Duda JE, Giasson BI (2008) Characterization of antibodies that selectively detect alpha-synuclein in pathological inclusions. *Acta Neuropathol* 116(1):37–46.

Supporting Information

Sacino et al. 10.1073/pnas.1321785111

SI Materials and Methods

Expression and Purification of Recombinant αS Proteins. Recombinant N-terminal truncated 21–140 human α-synuclein (αS) (with a Met codon added before amino acid 21), 71–82 deletion (Δ71–82) human αS, and full-length mouse αS were expressed and purified to homogeneity as previously described (1–3). The 21–140 human αS was shown to induce αS inclusion formation similar to full-length protein in cultured cells (4, 5) but provided the added advantage of being able to determine that inclusions are comprised of the endogenously expressed αS using N-terminal αS antibodies (6, 7). The Δ71–82 αS has a deletion in the middle of the hydrophobic region of αS that is required for amyloid formation and therefore lacks the ability to form or seed αS amyloid in vitro and in vivo under physiological conditions (1, 2, 4, 8).

Fibril Preparation of Recombinant αS for Injection. αS protein was assembled into filaments by incubation at 37 °C at 5 mg/mL in sterile PBS (Invitrogen) with continuous shaking at 1,050 rpm (Thermomixer R; Eppendorf) for 48 h. αS amyloid fibril assembly was monitored as previously described with K114 fluorometry (2, 9). αS fibrils were diluted in sterile PBS and treated by mild water bath sonication for 2 h at room temperature. These fibrils were tested for induction of intracellular amyloid inclusion formation as previously described (5). The Δ71–82 αS used for the current studies was not preincubated and is in the soluble form as previously described (1, 2). We have also recently shown that this same preparation of Δ71–82 αS cannot directly seed the formation of αS inclusions in primary neuronal culture. In contrast, the same preparation of fibrillar αS can seed inclusion formation very efficiently in those cultures (8).

Immunohistochemical Analysis. Mice were killed with CO_2 euthanization and perfused with PBS/heparin. The brain and spinal cord were then removed and fixed for at least 48 h in 70% ethanol/150 mM NaCl or neutral buffered formalin followed by paraffin infiltration. Paraffin-embedded tissue blocks were cut in 7-μm sections that were immunostained using previously described methods and immunocomplex visualization via chromogen 3,3′-diaminobenzidine (10). Sections also were counterstained with hematoxylin. All slides were scanned using an Aperio ScanScope CS (40× magnification; Aperio Technologies), and images of representative areas were taken using the ImageScope software (40× magnification; Aperio Technologies). Quantification of immunoreactivity for the levels of astrogliosis and microgliosis was accomplished using ImageScope software to measure the density of staining per area. Three independent regions were quantified per animal, and two animals were used per condition. The data are expressed as averaged immunoreactivity per area normalized to the control ± SEM. Stained tissue sections from untreated young (3 mo to 4 mo) M83 transgenic (Tg) mice without αS inclusion pathology were used as the baseline control.

Muscle Histology. Whole-mount flexor digitorum brevis muscles were placed into ice-cold PBS for less than 10 min to remove connective tissue and gently spread the muscle bundles using sharp forceps. Tissues were fixed with 4% paraformaldehyde in PBS for 20 min at room temperature, rinsed, and processed for immunostaining as described (11). Whole mounts were incubated in blocking buffer (PBS with 1% Triton X-100, 5% normal goat serum, and 1% BSA) overnight at 4 °C and then incubated in chicken anti-neurofilament-H (1:3,000; Encore Biotechnology) and mouse monoclonal anti-syntaptotagmin (1:1,000; Developmental Studies Hybridoma Bank) antibodies in diluting buffer for 24 h at 4 °C. Whole mounts were washed in PBS for 3 h, followed by incubation in Alexa-488 goat anti-chicken and Alexa-488 goat anti-mouse secondary antibodies and Alexa-594 α-bungarotoxin (all from Invitrogen) overnight at 4 °C. After washing for 3 h in PBS, samples were mounted on slides in ProLong Antifade mounting media (Invitrogen). Quantification of the neuromuscular junction (NMJ) integrity was assessed as a ratio of the number of innervated NMJs (seen by full colocalization of presynaptic axonal and postsynaptic acetylcholine receptor markers) (Fig. S6*A*) divided by the total number of postsynaptic receptor sites per field (Fig. S6*B*) in αS intramuscular (IM)-injected $M83^{+/-}$ Tg mice ($n = 10$) and age-matched, naive $M83^{+/-}$ Tg mice ($n = 10$).

Motor Neuron Counting. The entire lumbar region of each mouse spinal cord was paraffin-embedded and consecutive-sectioned (7 μm). These sections were deparaffinized and hydrated through a series of graded ethanol solutions. The sections were incubated in 0.1% Luxol fast blue solution at 56 °C overnight. After rinsing in distilled water, sections are differentiated in 0.05% lithium carbonate and 70% (vol/vol) ethanol. Sections were counterstained with cresyl violet solution for 6 min before differentiation in 95% (vol/vol) ethanol and dehydration. The number of motor neurons from every tenth section of the lumbar cord was then counted from phenotypic IM-injected M83 Tg mice ($n = 6$) and from native nontransgenic (nTg) mice ($n = 4$). The data were then expressed as a ratio of the average number of motor neurons in the lumbar spine of M83 Tg mice to nTg mice. This comparison was used because it has been previously shown that aged, symptomatic (paralyzed) M83 Tg mice show no loss of motor neuron counts compared with nTg mice (10).

Double-Labeling Immunofluorescence Analysis of Mouse Brain Tissue. Paraffin-embedded tissue sections were deparaffinized and hydrated through a series of graded ethanol solutions followed by 0.1 M Tris (pH 7.6). The sections were blocked with 5% dry milk/0.1 M Tris (pH 7.6) and were incubated simultaneously with combinations of primary antibodies diluted in 5% dry milk/0.1 M Tris (pH 7.6). After extensive washing, sections were incubated with secondary antibodies conjugated to Alexa 594 or Alexa 488 (Invitrogen). Sections were postfixed with formalin, incubated with Sudan Black, and stained with 5 μg/mL 4′,6-diamindino-2-phenylindole (DAPI). The sections were cover-slipped with Fluoromount-G (SouthernBiotech) and visualized using an Olympus BX51 microscope mounted with a DP71 Olympus digital camera to capture images.

Antibodies. pSer129/81A is a mouse monoclonal antibody that recognized αS phosphorylated at Ser129 (12). SNL-4 is a rabbit polyclonal antibody raised against a synthetic peptide corresponding to amino acids 2–12 of αS (6). Syn506 is an anti–N-terminal αS antibody that preferentially detects αS in pathological inclusions (7). Anti-p62 (SQSTM1; Proteintech), anti-glial fibrillary acidic protein (GFAP) (Promega), and anti-ionized calcium-binding adaptor molecule 1 (Iba-1) (DAKO) are rabbit polyclonal antibodies. Anti-choline acetyltransferase (CHAT) (Millipore) is a goat polyclonal antibody. Chicken polyclonal anti-neurofilament-H antibody was obtained from Encore Biotechnology and a mouse monoclonal anti-syntaptotagmin antibody was from the Developmental Studies Hybridoma Bank.

1. Giasson BI, Murray IV, Trojanowski JQ, Lee VMY (2001) A hydrophobic stretch of 12 amino acid residues in the middle of alpha-synuclein is essential for filament assembly. *J Biol Chem* 276(4):2380–2386.
2. Waxman EA, Mazzulli JR, Giasson BI (2009) Characterization of hydrophobic residue requirements for alpha-synuclein fibrillization. *Biochemistry* 48(40):9427–9436.
3. Greenbaum EA, et al. (2005) The E46K mutation in alpha-synuclein increases amyloid fibril formation. *J Biol Chem* 280(9):7800–7807.
4. Luk KC, et al. (2009) Exogenous alpha-synuclein fibrils seed the formation of Lewy body-like intracellular inclusions in cultured cells. *Proc Natl Acad Sci USA* 106(47): 20051–20056.
5. Waxman EA, Giasson BI (2010) A novel, high-efficiency cellular model of fibrillar alpha-synuclein inclusions and the examination of mutations that inhibit amyloid formation. *J Neurochem* 113(2):374–388.
6. Giasson BI, et al. (2000) A panel of epitope-specific antibodies detects protein domains distributed throughout human alpha-synuclein in Lewy bodies of Parkinson's disease. *J Neurosci Res* 59(4):528–533.
7. Waxman EA, Duda JE, Giasson BI (2008) Characterization of antibodies that selectively detect alpha-synuclein in pathological inclusions. *Acta Neuropathol* 116(1):37–46.
8. Sacino AN, et al. (2013) Conformational templating of α-synuclein aggregates in neuronal-glial cultures. *Mol Neurodegener* 8:17.
9. Crystal AS, et al. (2003) A comparison of amyloid fibrillogenesis using the novel fluorescent compound K114. *J Neurochem* 86(6):1359–1368.
10. Giasson BI, et al. (2002) Neuronal alpha-synucleinopathy with severe movement disorder in mice expressing A53T human alpha-synuclein. *Neuron* 34(4):521–533.
11. Valdez G, et al. (2010) Attenuation of age-related changes in mouse neuromuscular synapses by caloric restriction and exercise. *Proc Natl Acad Sci USA* 107(33):14863–14868.
12. Waxman EA, Giasson BI (2008) Specificity and regulation of casein kinase-mediated phosphorylation of alpha-synuclein. *J Neuropathol Exp Neurol* 67(5):402–416.

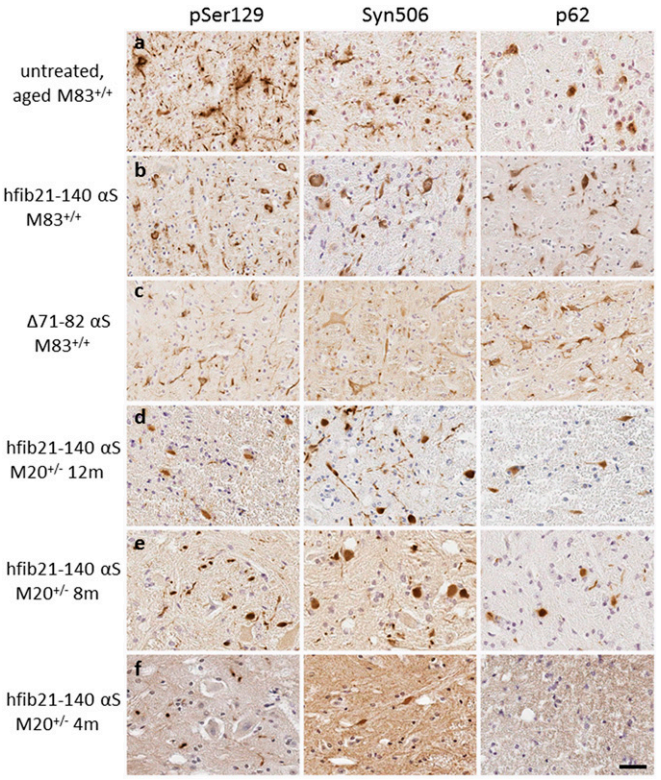

Fig. S1. αS pathology in injected M83$^{+/+}$ and M20$^{+/-}$ Tg mice is detectable with multiple markers for mature αS pathology. Representative images of brainstem tissue sections from a 15-mo-old, untreated M83$^{+/+}$ Tg mouse that developed motor impairments (*A*), an M83$^{+/+}$ Tg mouse that is 2 mo post-IM (biceps femoris muscle) injection with hfib21-140 αS (*B*), and an M83$^{+/+}$ Tg mouse that is 4 mo postinjection (biceps femoris muscle) with Δ71–82 αS (*C*); and cervical spinal cord tissue sections from M20$^{+/-}$ Tg mice that are 12 mo (*D*), 8 mo (*E*), and 4 mo (*F*) postinjection (biceps femoris muscle) hfib21-140 αS. Sections were stained with three separate markers for mature αS pathology: pSer129/81A, an antibody detecting αS inclusions that are hyperphosphorylated at Ser129 (1, 2); Syn506, an antibody that specially recognized the N terminus of αS (3); and p62, an antibody that nonspecifically recognizes intracellular protein aggregates (4). Each marker was able to detect αS pathology with similar staining densities in untreated and injected M83 Tg$^{+/+}$ mice, and 8 mo- and 12 mo-injected M20 Tg mice. In M20$^{+/-}$ Tg mice 4 mo after injection, inclusions were not stained with p62 antibodies. (Scale bar: 50 μm.)

1. Waxman EA, Giasson BI (2010) A novel, high-efficiency cellular model of fibrillar alpha-synuclein inclusions and the examination of mutations that inhibit amyloid formation. *J Neurochem* 113(2):374–388.
2. Waxman EA, Giasson BI (2008) Specificity and regulation of casein kinase-mediated phosphorylation of alpha-synuclein. *J Neuropathol Exp Neurol* 67(5):402–416.
3. Waxman EA, Duda JE, Giasson BI (2008) Characterization of antibodies that selectively detect alpha-synuclein in pathological inclusions. *Acta Neuropathol* 116(1):37–46.
4. Kuusisto E, Parkkinen L, Alafuzoff I (2003) Morphogenesis of Lewy bodies: dissimilar incorporation of alpha-synuclein, ubiquitin, and p62. *J Neuropathol Exp Neurol* 62(12):1241–1253.

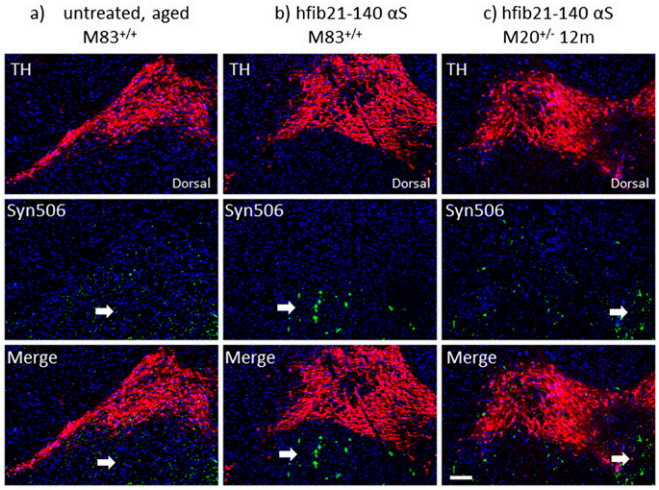

Fig. S2. αS inclusions in the substantia nigra region of $M83^{+/+}$ and $M20^{+/-}$ Tg mice are not found in dopaminergic neurons. Midbrain tissue sections from a 15-mo-old untreated, aged M83 $Tg^{+/+}$ mouse that developed motor impairments (*A*) and an $M83^{+/+}$ Tg mouse that is 2 mo postinjection (*B*) and an $M20^{+/-}$ Tg mouse that is 12 mo postinjection (*C*) with hfib21-140 αS. Double immunofluorescent labeling of dopaminergic neurons of the substantia nigra with tyrosine hydroxylase (TH; red) and Syn506 (green) shows that αS inclusions are predominantly found dorsal to the substantia nigra in the midbrain (arrows indicate the dorsal aspect of the midbrain region). Overlay images are shown in the bottom panels. (Scale bar: 100 μm.)

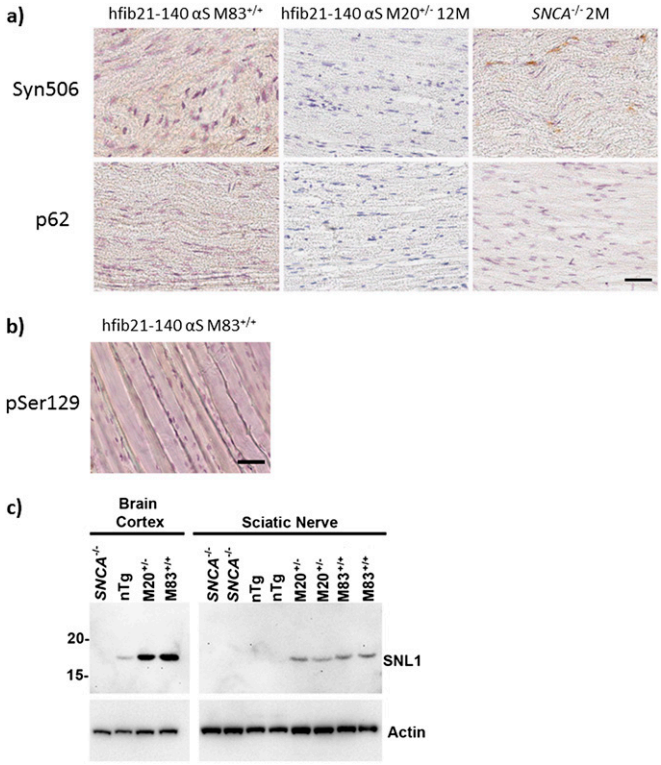

Fig. S3. αS inclusions are not present in the sciatic nerve or skeletal muscle of M83 or M20 Tg mice following IM injection of fibrillar αS. (*A*) Motor-impaired hfib21-140 αS-injected M83$^{+/+}$ and M20$^{+/-}$ Tg mice with robust CNS αS pathology did not exhibit any pathology in the sciatic nerve at the time of demise and revealed similar staining as untreated *SNCA*$^{-/-}$ controls. Similarly, no αS pathology could be detected in the sciatic nerve of M83$^{+/-}$ Tg mice injected with αS fibrils. pSer129 staining was not used to detect αS inclusion pathology in sciatic nerve due to cross-reactive staining with phosphorylated low molecular mass neurofilament subunit, which is abundant in white matter tracts (1). (*B*) No αS inclusion pathology was observed in the skeletal hind limb muscles of M83$^{+/+}$ Tg mice postinjection of hfib21-140 αS at the time when the mice were harvested. Similarly, no αS inclusion pathology was detected with antibody Syn 506 or in any M83$^{+/-}$ or M20$^{+/-}$ Tg IM-injected with fibrillar αS. (*C*) In both M83$^{+/+}$ and M20$^{+/-}$ Tg mice, αS expression is found in the sciatic nerve; however, expression is lower than in brain and it was not detected in nTg mice. Equal amounts (7.5 μg) of total SDS-soluble total protein extracts from the brain cortex or sciatic nerve of individual M20$^{+/-}$ and M83$^{+/+}$ Tg, nTg, and αS-null mice (SNCA$^{-/-}$) (2) were loaded on separate lanes of an SDS-polyacrylamide gel and analyzed by immunoblotting with antibody SNL1 that detects both murine and human αS (3) or an antibody (clone C4) (Millipore) to total actin as a loading control. The motilities of molecular mass markers are indicated on the left. (Scale bars: 100 μm.)

1. Sacino AN, et al. (2014) Amyloidogenic α-synuclein seeds do not invariably induce rapid, widespread pathology in mice. *Acta Neuropathol* 127(5):645–665.
2. Abeliovich A, et al. (2000) Mice lacking alpha-synuclein display functional deficits in the nigrostriatal dopamine system. *Neuron* 25(1):239–252.
3. Giasson BI, et al. (2000) A panel of epitope-specific antibodies detects protein domains distributed throughout human alpha-synuclein in Lewy bodies of Parkinson's disease. *J Neurosci Res* 59(4):528–533.

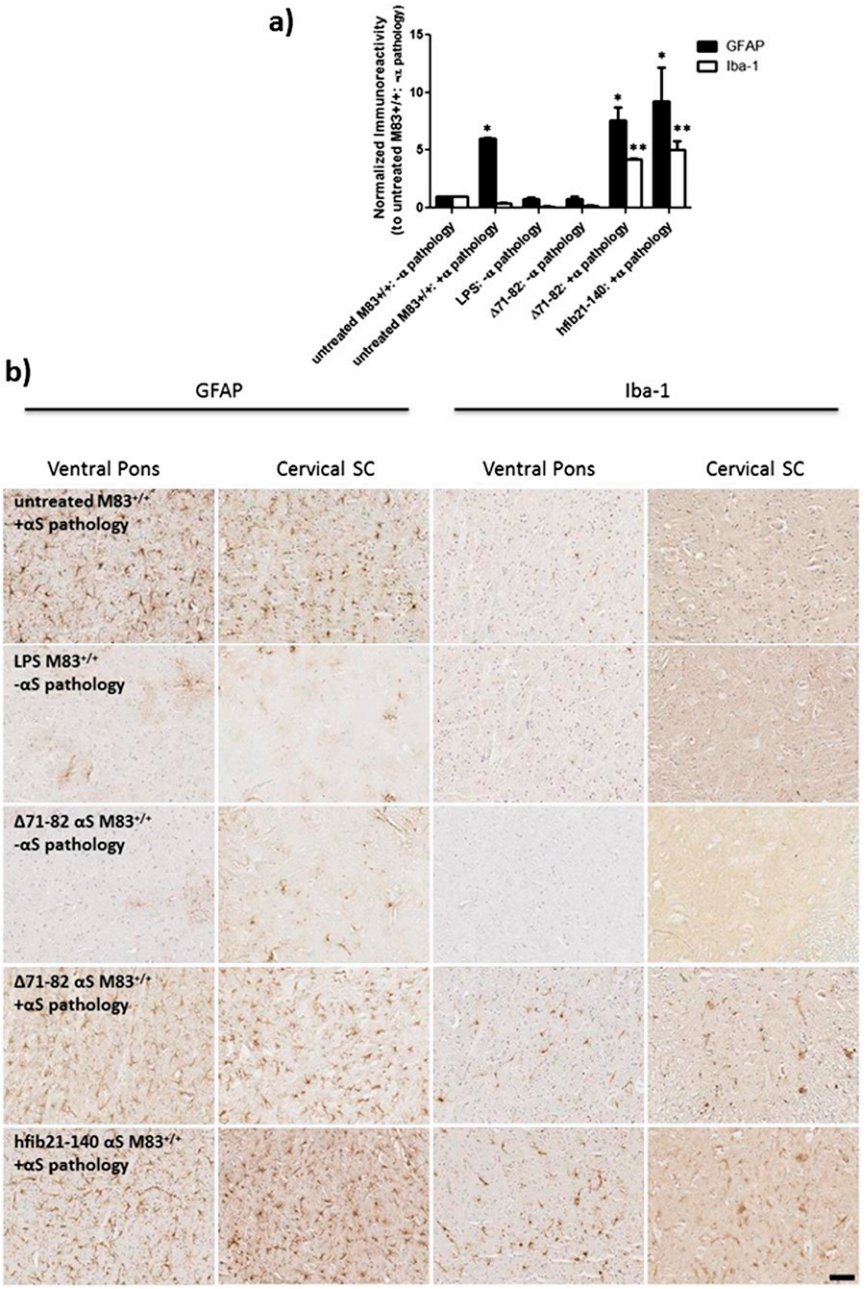

Fig. S4. Accelerated onset of astrogliosis and induction of microgliosis in M83$^{+/+}$ Tg mice IM-injected with Δ71–82 αS and hfib21-140 αS compared with untreated, aged M83$^{+/+}$ Tg mice. (*A*) For each condition, quantitative analyses of GFAP immunoreactivity, a marker of the astrogliosis, and Iba-1 immunoreactivity, a marker of microgliosis, per area were performed and normalized relative to the staining signal in untreated M83$^{+/+}$ Tg mice without αS inclusion pathology. M83$^{+/+}$ Tg mice IM-injected with either Δ71–82 αS or hfib21-140 αS and that develop robust αS CNS inclusion pathology demonstrated a six- to eightfold increase in the abundance of GFAP staining signal similar to that seen in untreated, aged M83$^{+/+}$ Tg mice that presented with αS inclusion pathology (associated with aging and motor impairment) (*$P < 0.001$). Mice IM-injected with αS protein and that developed CNS αS inclusion pathology also showed an approximately fivefold increase in Iba-1 staining signal, which was not seen in motor impairment untreated, aged M83$^{+/+}$ Tg mice (**$P < 0.001$). No quantitative increase in GFAP or Iba-1 staining was observed in M83$^{+/+}$ Tg mice IM-injected with LPS or Δ71–82 αS and that did not develop CNS αS inclusion pathology. (*B*) Representative images of ventral pons or cervical spinal cord tissue sections stained by immunohistochemistry (IHC) for GFAP or Iba-1. In untreated, aged M83$^{+/+}$ Tg mice with robust αS pathology in the pons and spinal cord, there is increased astrogliosis in the pons and gray matter of the spinal cord with limited microgliosis. M83$^{+/+}$ Tg mice IM-injected with 10 μg of LPS or 10 μg of Δ71–82 αS that has no αS inclusion pathology at 4 mo postinjection showed baseline levels of astrocytes and microglia in the pons and spinal cord. M83$^{+/+}$ Tg mice IM-injected with 10 μg of Δ71–82 αS or 10 μg of hfib21-140 αS that developed αS pathology demonstrated elevated astrogliosis and increased microgliosis in both these affected areas. (Scale bar: 100 μm.)

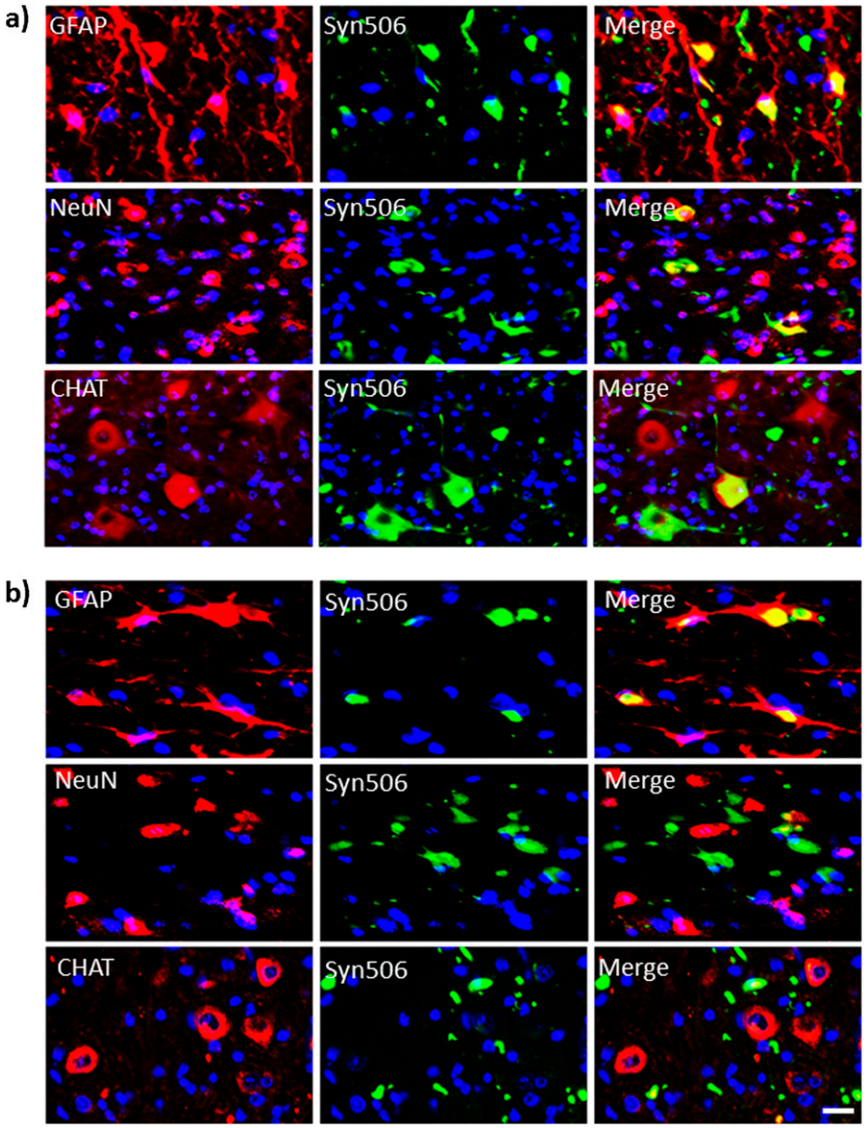

Fig. S5. αS inclusion pathology is found in multiple cell types postinjection of fib αS in both $M83^{+/+}$ and $M20^{+/-}$ Tg mice. Double immunofluorescence analysis of cervical spinal cord tissue from an $M83^{+/+}$ Tg mouse that is 2 mo postinjection (*A*) and an $M20^{+/-}$ Tg mouse that is 12 mo postinjection (*B*) of 10 μg of hfib21-140 αS. In $M83^{+/+}$ Tg mice, Syn506+ αS inclusions were found in both astrocytes (GFAP) and neurons (NeuN), particularly in motor neurons in the ventral horn of the spinal cord (CHAT). In $M20^{+/-}$ Tg mice, Syn506+ αS inclusions were frequently found in astrocytes and to a lesser extent in neurons; however, rarely were any αS inclusions found in motor neurons. Tissue sections were counterstained with DAPI (blue). (Scale bar: 50 μm.)

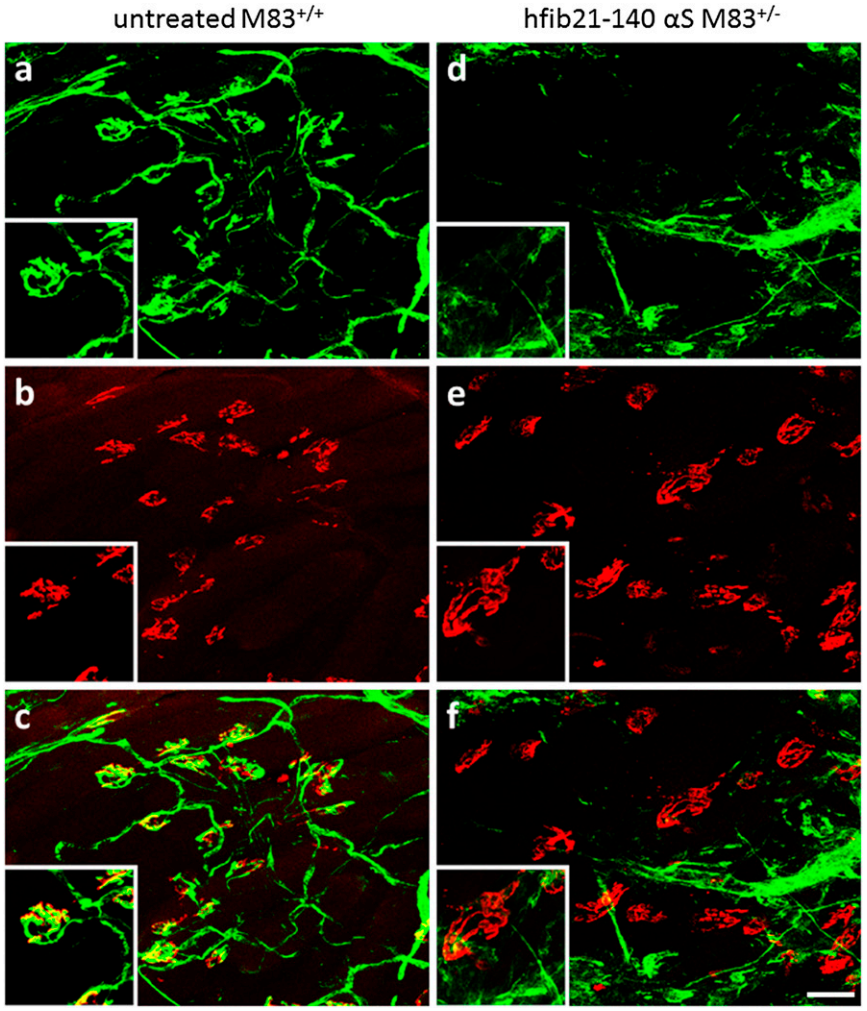

Fig. S6. Loss of intact NMJ in M83$^{+/-}$ Tg mice after injection of 10 μg of hfib21-140 αS. Double-immunofluorescence analysis of the digitorum brevis muscles of untreated M83$^{+/+}$ Tg mice and injected M83$^{+/-}$ Tg mice was used to detect the presynaptic motor neuron axon (neurofilament H and syntaptotagmin; green; *A* and *D*) and the postsynaptic acetylcholine receptor (α-bungarotoxin; red; *B* and *E*) of the NMJ. In the native M83$^{+/+}$ Tg mice, the NMJs were fully innervated as shown by colocalization of motor neuron axonal markers with postsynaptic receptors (*C*). However, in the M83$^{+/-}$ Tg mice IM injected with hfib21-140 αS and exhibiting a progressive, degenerative motor phenotype, there was dramatic withdrawal of motor neuron axons from the postsynaptic sites (*F*). (Scale bar: *A–F*, 50 μm; *Insets*, 25 μm.)

Table S1. Summary of M83 Tg mice injected with αS proteins and LPS control

Strain	Inoculum	Muscle site of injection	No. of mice	Median survival, dpi	Phenotype	Pathology
M83$^{+/+}$ (A53T αS)	Bilateral hfib21-140-αS (5 μL of 2 mg/mL)	Biceps femoris	15	77	12 of 15 with foot drop/paralysis*	12 of 15 with robust αS pathology*
M83$^{+/+}$ (A53T αS)	Bilateral mfib-αS (5 μL of 2 mg/mL)	Biceps femoris	7	53	7 of 7 with foot drop/paralysis	7 of 7 with robust αS pathology
M83$^{+/+}$ (A53T αS)	Unilateral mfib-αS (5 μL of 2 mg/mL)	Gastrocnemius	9	56	8 of 9 with foot drop/paralysis[†]	8 of 9 with robust αS pathology[†]
M83$^{+/+}$ (A53T αS)	Bilateral Δ71–82 αS (5 μL of 2 mg/mL)	Biceps femoris	11	120	2 of 11 with foot drop/paralysis[‡]	5 of 11 with αS pathology[§]
M83$^{+/+}$ (A53T αS)	Bilateral LPS (5 μL of 5 mg/mL)	Biceps femoris	5	Harvested at 123 dpi	0 of 5 with foot drop/paralysis	0 of 5 with αS pathology
M83$^{+/-}$ (A53T αS)	Bilateral hfib21-140-αS (5 μL of 2 mg/mL)	Gastrocnemius	10	111	10 of 10 with foot drop/paralysis	10 of 10 with robust αS pathology
M83$^{+/-}$ (A53T αS)	Unilateral mfib-αS (5 μL of 2 mg/mL)	Gastrocnemius	10	129	10 of 10 with foot drop/paralysis	10 of 10 with robust αS pathology
M83$^{+/-}$ (A53T αS)	Unilateral mfib-αS (5 μL of 2 mg/mL) SNT[¶]	Gastrocnemius	7	Undefined[‖]	3 of 7 mice with foot drop/paralysis**	3 of 7 mice with robust αS pathology**

M83 Tg mice received injections at 2 mo of age. See Fig. 2 for pathology distribution.
*Two mice died suddenly without an observed phenotype and were not available to analyze for αS pathology.
[†]One mouse died suddenly without an observed phenotype and was not available to analyze for αS pathology.
[‡]Two of these mice had a similar foot drop phenotype and extensive hind limb paralysis as mice injected with fib αS, and an additional four mice were moribund with more subtle muscle weakness, but without obvious foot drop or paralysis. They were killed upon veterinary recommendation.
[§]Two of these mice had widespread αS pathology as described in Fig. 2*C*. Three additional mice without a phenotype had αS pathology in the same area, but less abundant.
[¶]SNT, sciatic nerve transection.
[‖]Four mice in the cohort are still living with no sign of any degenerative phenotype.
**See Fig. 3.

Table S2. Summary of M20 Tg mice injected with αS proteins and PBS control

Strain	Inoculum	Muscle site of injection	No. of mice	Harvest time point, dpi	Phenotype	Pathology
M20$^{+/-}$ (WT αS)	Bilateral PBS (5 μL)	Biceps femoris	5	360	0 of 5 with foot drop/paralysis	0 of 5 with αS pathology
M20$^{+/-}$ (WT αS)	Bilateral Δ71–82 αS (5 μL of 2 mg/mL)	Biceps femoris	5	360	0 of 5 with foot drop/paralysis	1 of 5 with rare αS inclusions in spinal cord*
M20$^{+/-}$ (WT αS)	Bilateral hfib21-140-αS (5 μL of 2 mg/mL)	Biceps femoris	7	120	0 of 7 with foot drop/paralysis	1 of 7 with sparse αS inclusions in spinal cord*
M20$^{+/-}$(WT αS)	Bilateral hfib21-140-αS (5 μL of 2 mg/mL)	Biceps femoris	5	240	0 of 5 with foot drop/paralysis	5 of 5 with moderate spinal cord and brain αS pathology
M20$^{+/-}$(WT αS)	Bilateral hfib21-140-αS (5 μL of 2 mg/mL)	Biceps femoris	5	360	0 of 5 with foot drop/paralysis	5 of 5 with moderate spinal cord and brain αS pathology

M20 Tg mice received injections at 2 mo of age. See Fig. 4 for pathology distribution.
*These inclusions in spinal cord were detected with αS antibodies but not antibodies to the general inclusion marker p62 (Fig. 4 and Fig. S1).

Table S3. Summary of IM-injected nTg and *SNCA*$^{-/-}$ mice

Strain	Inoculum	Muscle site of injection	No. of mice	Harvest time point, dpi	Phenotype	Pathology
nTg	Bilateral hfib-αS (5 μL of 2 mg/mL)	Biceps femoris	5	360	0 of 5 with foot drop/paralysis	0 of 5 with αS pathology
nTg	Bilateral mfib-αS (5 μL of 2 mg/mL)	Biceps femoris	5	360	0 of 5 with foot drop/paralysis	0 of 5 with αS pathology
SNCA$^{-/-}$	Bilateral hfib-αS (5 μL of 2 mg/mL)	Biceps femoris	7	360	0 of 5 with foot drop/paralysis	0 of 5 with αS pathology

nTg and *SNCA*$^{-/-}$ mice received injections at 2 mo of age.

Movie S1. Bilateral hind limb foot drop and hind leg weakness in an M83$^{+/+}$ Tg mouse at 2 mo post IM injection of hfib21-140 αS. The foot drop progressed to paralysis and a moribund state within a week.

Movie S1